


## Predicting Bubble Fragmentation in Superfluids

Jake McMillan<sup>1</sup>, Thomas A. Flynn<sup>1</sup>, and Ryan Doran<sup>1</sup>

*Joint Quantum Centre (JQC) Durham–Newcastle, School of Mathematics, Statistics and Physics,  
Newcastle University, Newcastle upon Tyne, NE1 7RU, United Kingdom*

 (Received 8 November 2023; revised 6 June 2024; accepted 24 July 2024; published 29 August 2024)

In classical fluids, the Weber number is a dimensionless parameter that characterizes the flow of a multiphase fluid. The superfluid analogy of a classical multiphase fluid can be realized in a system of two or more immiscible Bose-Einstein condensates. These superfluid mixtures have been shown to display a wider variety of exotic dynamics than their single component counterparts. Here we systematically study the dynamics of a binary immiscible Bose-Einstein condensate in two dimensions, where a small bubble of the second component is used to “stir” the first component. We begin by rigorously mapping out the critical velocity for vortex shedding as a function of the size of the bubble, in analogy to the critical velocity of a laser spoon. Observing that the dynamics of the system depend on the initial size and velocity of the bubble, we then show that a dimensionless parameter with the same form as the Weber number accurately predicts the resulting bubble fragmentation.

DOI: [10.1103/PhysRevLett.133.093403](https://doi.org/10.1103/PhysRevLett.133.093403)

**Introduction**—From rainfall [1] to liquid jets [2] and the smelting of liquid metals [3], the dynamics of a wide variety of flows that consist of two or more fluids with an interface can be characterized by the Weber number [4]. For classical multiphase flows (i.e., droplets of oil contained in water flow), the Weber number is given by

$$\text{We} = \frac{\rho v^2 l}{\sigma}, \quad (1)$$

where  $\rho$  is the density of the fluid,  $v$  is the characteristic velocity of the droplet in the fluid,  $l$  is the characteristic size of the droplet, and  $\sigma$  is the surface tension at the interface of the droplet. In general, multiphase flows are nontrivial systems that exhibit complex dynamics. The advantage of the Weber number is that it is a dimensionless parameter based on a small number of observables that broadly characterizes the dynamics of the system, without the need for extensive numerical analysis or experimental measurements. In a flow with a very small Weber number, a droplet will retain its original shape. As the Weber number increases in magnitude, vibrational modes will appear on the droplet, leading to deformations and eventually the fragmentation of the droplet. For very large Weber numbers, a catastrophic break-up mode will occur [5], where the original droplet will break into smaller droplets, and these droplets will break into smaller droplets still.

The superfluid analogy of multiphase fluids have been realized in mixtures of atomic Bose Einstein condensates (BECs), where the two (or more) components are coupled, and the components may be miscible or immiscible, depending on the interspecies and intraspecies interaction strengths [6]. BEC mixtures can be formed in the same atomic species [7–16], different isotopes of the same atomic species [17,18], and with different atomic species [19–22]. By comparison with single component BECs, two-component BECs have been shown to exhibit an exotic variety of both steady state solutions [6,23–31], and dynamics [32–36]. In addition, recent works on superfluid mixtures have uncovered a rich vein of counterparts to instabilities found in classical fluids. In mixtures that have a mass imbalance, analogies to the Richtmyer-Meshkov [37] and Rayleigh-Taylor instabilities have been predicted [38,39], while for superfluid systems subject to long-range dipole interactions, ferrofluid instabilities such as the Rosensweig [40] and fingering [41] instability have been predicted and experimentally observed. These results hint at the diverse range of instabilities available in two-component superfluids [42].

While superfluids are characterized by their frictionless flow about an obstacle, it has been shown that dragging an obstacle through a superfluid faster than a critical velocity will nucleate vortices [43], and increasing the speed of the obstacle further still will lead to a turbulent system [44,45]. While there has been much focus on determining the critical velocity as a function of obstacle shape [46,47] and condensate temperature [48,49], these studies are limited to the case of an external potential acting as an obstacle, which acts as a “laser spoon” in creating a well-defined region of depleted condensate density. In the

---

*Published by the American Physical Society under the terms of the Creative Commons Attribution 4.0 International license. Further distribution of this work must maintain attribution to the author(s) and the published article's title, journal citation, and DOI.*

absence of an imposed obstacle, it is still possible to create an area of depleted density, by adding an immiscible second component to the system [8,10], which is subject to arbitrary spatiotemporal control [50]. Previous theoretical work on immiscible binary condensates has observed that a bubble of component 2 will deform and then shed vortices in component 1 as it is subjected to a linear forcing potential [51]. However, it is not possible to identify a critical velocity at which the bubble will shed vortices into the other component, owing to the setup of the potential.

In this work, by controlling the imposed velocity profile of the bubble, we systematically study the bubble's critical velocity as a function of its size. The wake of the bubble is determined both by its size and its initial velocity. Small bubbles traveling at low speeds are trailed by laminar flow. As either the bubble's velocity or size is increased, one vortex–antivortex pair is shed, the cores of which are filled by some of the atoms that originally formed the bubble. Large bubbles traveling at high speeds shed many vortices, leaving a dense wake. Most notably, we observe a dynamic similarity between the wakes of bubbles with different sizes and velocities; motivated by previous studies into dynamic similarities [52], we identify a dimensionless quantity that parametrizes the resulting dynamics of the system. This quantity, the superfluid Weber number,  $We_s$ , is based on the classical Weber number, Eq. (1), and is determined by the number of atoms in the bubble and the interspecies interaction strength; two highly controllable experimental parameters. The Weber number also has the advantage that it characterizes the dynamics of the system based on the initial configuration, removing the need to disturb the system during its evolution (i.e., to perform time-of-flight imaging) to visualize the flow. We show that the value of this number accurately predicts the onset of quantum turbulence, via the irregular shedding of filled vortices.

*Governing equations and numerical implementation*—We consider a binary system of weakly interacting BECs in the zero temperature limit. This consists of a majority component, with macroscopic wave function  $\psi_1$  and atomic mass  $m_1$ , which contains a “bubble” of a second component, with macroscopic wave function  $\psi_2$  and atomic mass  $m_2$ . For simplicity, we consider a homogeneous system with no in-plane trapping potential on either species. Such a system is accurately described by a 2D coupled Gross-Pitaevskii Equation (GPE)

$$i\hbar \frac{\partial \psi_1}{\partial t} = \left[ -\frac{\hbar^2}{2m_1} \nabla^2 + u_{11}|\psi_1|^2 + u_{12}|\psi_2|^2 \right] \psi_1, \quad (2a)$$

$$i\hbar \frac{\partial \psi_2}{\partial t} = \left[ -\frac{\hbar^2}{2m_2} \nabla^2 + u_{12}|\psi_1|^2 + u_{22}|\psi_2|^2 \right] \psi_2, \quad (2b)$$

where sufficient trapping is applied in the  $z$  axis to prevent excitations out of the plane [53]. We can cast Eqs. (2a) and (2b) in dimensionless form by working in the characteristic

units of the majority component: background density  $n_{1,0}$ , healing length  $\xi_1 = \hbar/\sqrt{m_1 u_{11} n_{1,0}}$ , characteristic time,  $\tau = \hbar/(u_{11} n_{1,0})$ , and speed of sound  $c_1 = \sqrt{u_{11} n_{1,0}/m_1}$ . In the remainder of this Letter, we will normalize component 1 to  $N_1$  and refer to this as the majority component, while component 2 is normalized to  $N_2$ . The value of  $N_1$  is chosen so that the background density of component 1 is approximately unity across our computational domain,  $n_{1,0} \approx 1$ , and we vary the population of the second component,  $N_2$ , while fixing the requirement for the density of the bubble to be unity in the bulk,  $n_{2,0} \approx 1$  [54]. We suppose that our binary system comprises homonuclear systems with equal masses,  $m_1 = m_2 = m$ , and equal intraspecies interaction parameters,  $u_{11} = u_{22}$ . This, coupled with the fact that the background density of each species is unity in the bulk, means that the healing length and speed of sound is identical in each component, and as such we will omit the subscripts on the healing length  $\xi$ , characteristic time  $\tau$ , and speed of sound  $c$ .

The formation of a bubble of the second component is a result of the immiscibility criterion for a homogeneous system [26], which constrains the interspecies interaction strength  $u_{12}$  as  $u_{12}^2 > u_{11}u_{22}$ . Having set the intraspecies scattering lengths to be identical, and taking  $u_{12} > 0$ , we can write this constraint as  $g_{12} = u_{12}/\sqrt{u_{11}u_{22}} > 1$ , and we will report values of  $g_{12}$  in the remainder of this Letter.

We solve the coupled GPE, Eqs. (2a) and (2b), using an adaptive RK45 method with a tolerance of  $10^{-8}$ , implemented using XMDS2 [55]. We do this on a computational grid that is discretized to have 2 numerical grid points per healing length, typically on a grid of size  $256\xi \times 128\xi$ ; where the size of the bubble becomes comparable to the size of this computational domain, we double the linear size. In order to initialize the system, we perform a Wick rotation  $t_i = it$  and evolve up to  $t_i = 100\tau$ , renormalizing both components after each step. This “imaginary time” propagation is a well-established method to obtain the lowest energy state of a system [56]. Once we have obtained the ground state, we impose a phase gradient in the  $x$  direction on the bubble, which is responsible for the initial velocity boost, before evolving the system in real time.

*The critical velocity*—Unlike the case of an obstacle that is imposed via an external potential [46–49], a system that is “stirred” using an immiscible second component does not have a well-defined zero-density region, since the second component can deform from its initial shape. This means that the critical velocity for vortex nucleation in the wake of the bubble cannot be predicted analytically using Landau's criterion [57], and so we determine the critical velocity numerically, as previous works have done for the case of an externally imposed barrier [46,47]. The vortices are quantized due to the superfluid nature of the system.

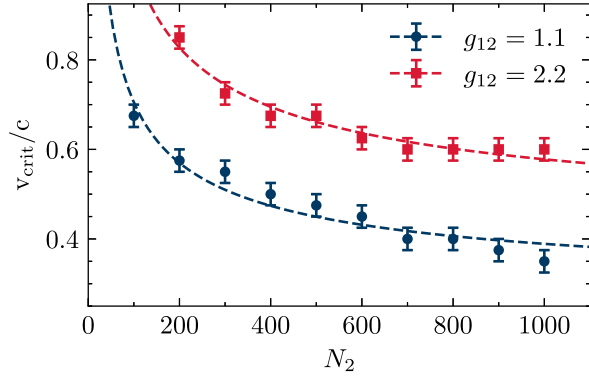


FIG. 1. The critical velocity,  $v_{\text{crit}}$  of the bubble containing  $N_2$  atoms, where the interspecies interaction strengths are  $g_{12} = 1.1$  (blue) and  $g_{12} = 2.2$  (red). The error bars indicate the discrete steps in the initial velocities. Dashed lines indicate the fitted curves given by Eq. (3).

The results of the vortex detection are presented in Fig. 1. Since the characteristic diameter of the bubble  $l$  scales as  $\sqrt{N_2}$ , we would expect that the critical velocity for vortex nucleation,  $v_{\text{crit}}$ , will decrease with the number of atoms in the bubble; this is consistent with previous studies for external stirring potentials [43,45,46,52]. Given the qualitative similarities between the immiscible bubble and a stirring potential, we fit an empirical model for the critical velocity,

$$\frac{v_{\text{crit}}}{c} = \frac{a}{\sqrt{N_2}} + b, \quad (3)$$

where  $b$  corresponds to the ‘‘Eulerian limit’’ of very large obstacles [58]. For  $g_{12} = 1.1$  we obtain  $a = 4.623 \pm 0.449$  and  $b = 0.243 \pm 0.024$ , while for  $g_{12} = 2.2$  we obtain  $a = 6.376 \pm 0.523$  and  $b = 0.376 \pm 0.024$ . The form of this fit has previously been used to determine the critical velocity for vortex shedding behind a stirring cylinder with a fixed width [46,48,59]. As  $N_2$  increases, the width of the initial bubble increases, and the critical velocity will decrease, asymptotically approaching the corresponding Eulerian limit for a given  $N_2$ . The effect of increasing  $g_{12}$  is to increase the repulsion between the bulk of the majority component and the bubble; this increases the critical velocity of the bubble in analogy with the increase in critical velocity of a hard-walled potential compared to a soft-walled potential [60].

*Characterizing the resulting dynamics*—While the critical velocity of a bubble containing  $N_2$  atoms of an immiscible second component has a likeness to vortex shedding from a dragged laser spoon, the bubble is not a fixed obstacle, and is able to deform or fragment over the lifetime of the experiment. Studies of two-component classical flows observe a number of ‘‘break-up’’ modes of the droplet, termed vibrational, bag, multimode, sheet-thinning, and catastrophic [5]. In a system of two

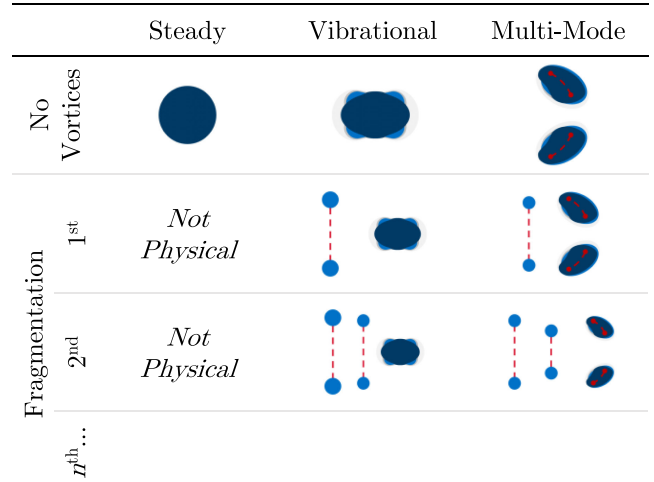


FIG. 2. A schematic of the dynamics of a bubble. From states with no vortex shedding, row 1, to states that fragment into 1 vortex–antivortex pair, row 2, to 2 vortex–antivortex pairs, row 3, and so on. Columns indicate the behavior of the original bubble.

immiscible superfluids, we are also able to identify a range of characteristic behaviors, which we categorize based on the long-term behavior of the fluid parcel that originated from the bubble and the number of vortex pairs that are shed in the wake of this parcel. A schematic of these dynamics can be found in Fig. 2.

For very low velocities, we observe a ‘‘steady’’ state where the fluid parcel is relatively unchanged from the original bubble (Fig. 2, top left), although any imposed velocity will lead to a ‘‘sloshing’’ motion (see the example movies of the dynamics in the Supplemental Material [61]). As the velocity of the bubble is increased, the surface tension at the interface gives rise to vibrational modes in the fluid parcel, similar to the surface modes observed in trapped BECs [62] (Fig. 2, top middle). The excitation spectrum of waves at the interface of two BECs has previously been studied [27]. As the velocity increases further (or  $N_2$  is increased), the vibrational modes of the bubble have sufficient energy that they are able to overcome the surface tension associated with the immiscibility condition, and the bubble breaks into two or more smaller parcels without forming vortices; this is the multimode phase (Fig. 2, top right).

As the velocity is increased beyond the critical velocity for a given  $N_2$ , we begin to observe fragmentation. The response of the superfluid system to this highly non-equilibrium state is to shed an even number of oppositely charged vortices. The 1st fragmentation occurs when a single vortex–antivortex pair is shed from the leading fluid parcel. The cores of this vortex–antivortex pair are filled with some of the second component, and the leading fluid parcel, which is now smaller than the original bubble, is then either in the vibrational or multimode state (Fig. 2, second row).

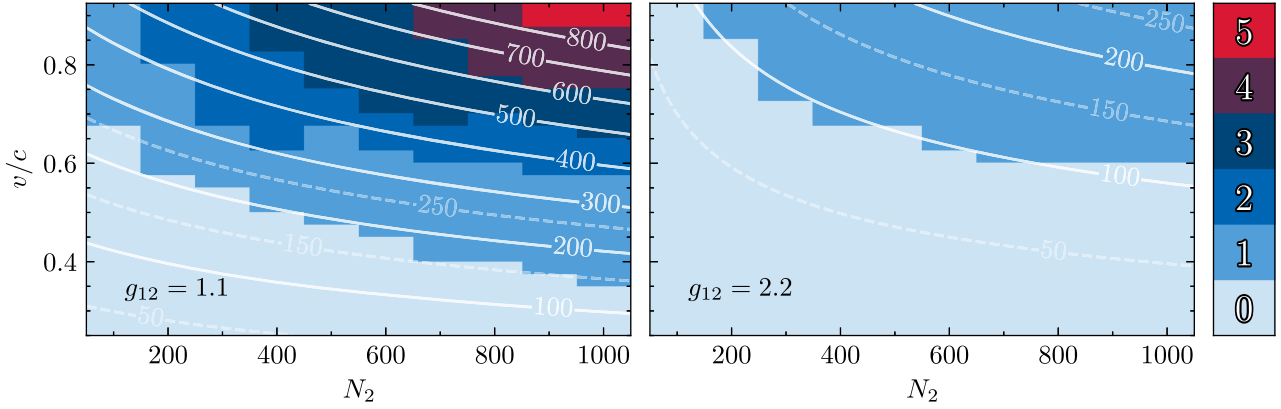


FIG. 3. Characterization of the dynamics for a system with  $g_{12} = 1.1$ , left, and  $g_{12} = 2.2$ , right. The color axis indicates the observed number of vortex–antivortex pairs that are shed over the lifetime of the simulation, the  $n$ th fragmentation. The contours are given by the superfluid Weber number, Eq. (4). Example movies of the dynamics are available in the Supplemental Material [61].

As the velocity is increased further still, and particularly for larger  $N_2$ , we observe recursive fragmentation events (see Fig. 2, third row). This occurs when the initial fluid bubble fragments by shedding one filled vortex–antivortex pair, but the remaining fluid parcel is still energetically unstable to the shedding of further vortices, and so a second filled vortex–antivortex pair is shed. We refer to this as 2nd fragmentation. For sufficiently large velocities and  $N_2$ , we can observe  $n$ th fragmentation of the initial bubble. On each occasion, a filled vortex–antivortex pair is shed from the leading fluid parcel, reducing the size of the leading fluid parcel, which will either continue to shed filled vortex–antivortex pairs, or it will enter one of the vibrational or multimode states. The recursive pattern of vortex shedding and bubble deformation is due to the superfluid nature of the system—the response of a given bubble to an imposed velocity is to shed vortex–antivortex pairs [60], due to the fact that vorticity is quantized in a superfluid, and the bubble is depleted after each shedding event, we see a reduced number of dynamical states compared to the classical case.

Having observed that the recursive nature of the bubble dynamics depends on the initial bubble velocity and initial bubble size, it would be useful to be able to predict the bubble dynamics based on some initial parameters. This leads us to a superfluid analog to the classical Weber number, Eq. (1). By approximating the density distribution of the two components to have hyperbolic tanh profiles [27], we can derive the surface tension at the interface of the two fluids to be  $\sigma = \xi P_0 \sqrt{g_{12} - 1} \tanh[\sqrt{N_2(g_{12} - 1)}/6\pi] / 4\sqrt{6}$ , where  $P_0 = u_{11} n_{1,0}^2 / 2$  is the pressure (the full derivation can be found in the Supplemental Material [61]). We can think of the surface tension as the energy required to deform the density of the components away from a homogeneous profile [28]; such a deformation is required by the immiscibility condition of the system, and for a unit area of interface will increase with  $g_{12}$ . This leads

to the Weber number for a binary system of immiscible superfluids, which is

$$\text{We}_s = \frac{8\sqrt{6}\rho v^2 \xi}{\sqrt{\pi}} \sqrt{\frac{N_2}{g_{12} - 1}} \coth \left[ \sqrt{\frac{N_2(g_{12} - 1)}{6\pi}} \right], \quad (4)$$

where  $\rho$  is the background density of the majority fluid,  $v$  is the initial velocity of the bubble, and  $l$  is the characteristic size of the bubble, which we approximate as  $l = \xi \sqrt{N_2/\pi}$ . The precise experimental control over the interaction parameter  $g_{12}$  and high-precision measurements of the atom number  $N_2$  are the hallmark of a superfluid formed of an ultracold quantum gas, and we see that these are the most prominent variables in the superfluid Weber number.

Our observed dynamics are presented in Fig. 3, along with the predictions of the superfluid Weber number, for each interspecies interaction strength. Although we would expect that the dynamics of any given individual realization will be subject to small fluctuations about the value predicted by Eq. (4), we see that the contours of the superfluid Weber number are in good agreement with the different regimes of bubble breakup. In particular, we see that  $100 \lesssim \text{We}_s \lesssim 150$  indicates a transition from no fragmentation, to 1st fragmentation. The presence of vortices in the system associated with fragmentation indicates the breakdown of superfluidity, and the transition of the system to a turbulent state [60,63,64]. In the case where  $g_{12} = 1.1$ , we see a wide range of dynamics, from no fragmentation (light blue), up to 5th fragmentation, which has a superfluid Weber number  $\text{We}_s \gtrsim 800$ . The dynamics of the system for this large superfluid Weber number is characterized by a large number of filled vortices, which is an inherently chaotic system that contains large velocity gradients; as  $\text{We}_s$  is increased further, these systems will become turbulent, as has been seen experimentally in one component [45]. This transition to turbulence takes place

when the dimensionless Weber number is an order of magnitude greater than the Weber number associated with the 1st fragmentation. We see the best agreement between the prediction of the superfluid Weber number and the ensuing dynamics of the system occurs at larger  $N_2$ ; this is because the approximation of the density profile of the two components is more accurate in this regime. In the case where  $g_{12} = 2.2$ , we are limited to 1st fragmentation for the values of  $N_2$  that we consider—this is due to the stronger immiscibility condition associated with the higher  $g_{12}$  preventing the initial bubble from breaking up, other than at high velocity or large bubble size. The superfluid Weber number correctly predicts that this will be the case.

**Conclusions**—For a binary system of immiscible superfluids, we have systematically determined the critical velocity for vortex shedding by a bubble of the second component. Such a system would be relatively easy to realize using current experimental setups, for example, by making use of DMDs [50]. We have then studied the resulting dynamics, and we have observed that they can be characterized by the number of vortices that are shed, and the behavior of the fluid parcel that remains from the bubble. Importantly, since vorticity is quantized, the dynamics are recursive—the bubble undergoes  $n$  fragmentation events (shedding  $n$  vortex–antivortex pairs) before reaching a vibrational or multimode state. The dynamics of the bubble wake depend on the initial velocity of the bubble, and the size of the bubble; we have shown that this wake can be characterized by a dimensionless parameter, the superfluid Weber number  $We_s$ , which resembles the form of a Weber number in classical multiphase flows, Eq. (1). Like the classical Weber number, the superfluid Weber number parameterises the dynamics of the system, and is a useful starting point to predict the nature of the resulting flow, with steady or vortex-free flow taking place when  $We_s \ll 100$ , the shedding of one vortex–antivortex pair occurring at  $100 \lesssim We_s \lesssim 150$ , and 5th fragmentation state occurs at  $We_s \gtrsim 800$ . Such dynamic similarities suggest that the superfluid Weber number may be applicable to a wide variety of superfluid systems, from binary immiscible Bose-Einstein condensates, to systems containing multiple phases of liquid helium. Excitingly, we have seen that the superfluid Weber number is particularly good when  $N_2$  is large or  $g_{12}$  is strong, the regime predicted to exhibit new forms of superfluid turbulence that are unavailable in one-component systems.

**Acknowledgments**—We thank Professor Nick Parker for helpful discussions during the preparation of this Letter. This work made use of the Rocket HPC facility at Newcastle University. J.M. thanks Newcastle University for a Vacation Research Scholarship. T. A. F. acknowledges support from the UK Engineering and Physical Sciences Research Council, Grant No. EP/T517914/1; R. D. is

supported by the UK Engineering and Physical Sciences Research Council, Grant No. EP/X028518/1.

**Data availability**—The data presented in this Letter are available from the corresponding author upon reasonable request.

- 
- [1] E. Villermaux and B. Bossa, *Nat. Phys.* **5**, 697 (2009).
  - [2] C. Varga, J. Lesheras, and E. Hopfinger, *J. Fluid Mech.* **497**, 405 (2003).
  - [3] T. Haas, C. Schubert, M. Eickhoff, and H. Pfeifer, *Metals* **11**, 664 (2021).
  - [4] E. Michaelides, C. Crowe, and J. Schwarzkopf, *Multiphase Flow Handbook*, 2nd ed (CRC Press, Taylor & Francis Group, Boca Raton, 2017).
  - [5] D. R. Guildenbecher, C. López-Rivera, and P. E. Sojka, *Exp. Fluids* **46**, 371 (2009).
  - [6] H. Pu and N. P. Bigelow, *Phys. Rev. Lett.* **80**, 1130 (1998).
  - [7] C. J. Myatt, E. A. Burt, R. W. Ghrist, E. A. Cornell, and C. E. Wieman, *Phys. Rev. Lett.* **78**, 586 (1997).
  - [8] D. S. Hall, M. R. Matthews, J. R. Ensher, C. E. Wieman, and E. A. Cornell, *Phys. Rev. Lett.* **81**, 1539 (1998).
  - [9] M. R. Matthews, B. P. Anderson, P. C. Haljan, D. S. Hall, C. E. Wieman, and E. A. Cornell, *Phys. Rev. Lett.* **83**, 2498 (1999).
  - [10] H.-J. Miesner, D. M. Stamper-Kurn, J. Stenger, S. Inouye, A. P. Chikkatur, and W. Ketterle, *Phys. Rev. Lett.* **82**, 2228 (1999).
  - [11] P. Maddaloni, M. Modugno, C. Fort, F. Minardi, and M. Inguscio, *Phys. Rev. Lett.* **85**, 2413 (2000).
  - [12] G. Delannoy, S. G. Murdoch, V. Boyer, V. Josse, P. Bouyer, and A. Aspect, *Phys. Rev. A* **63**, 051602(R) (2001).
  - [13] V. Schweikhard, I. Coddington, P. Engels, S. Tung, and E. A. Cornell, *Phys. Rev. Lett.* **93**, 210403 (2004).
  - [14] K. M. Mertes, J. W. Merrill, R. Carretero-González, D. J. Frantzeskakis, P. G. Kevrekidis, and D. S. Hall, *Phys. Rev. Lett.* **99**, 190402 (2007).
  - [15] R. P. Anderson, C. Ticknor, A. I. Sidorov, and B. V. Hall, *Phys. Rev. A* **80**, 023603 (2009).
  - [16] S. Tojo, Y. Taguchi, Y. Masuyama, T. Hayashi, H. Saito, and T. Hirano, *Phys. Rev. A* **82**, 033609 (2010).
  - [17] E. G. M. van Kempen, S. J. J. M. F. Kokkelmans, D. J. Heinzen, and B. J. Verhaar, *Phys. Rev. Lett.* **88**, 093201 (2002).
  - [18] S. B. Papp, J. M. Pino, and C. E. Wieman, *Phys. Rev. Lett.* **101**, 040402 (2008).
  - [19] G. Ferrari, M. Inguscio, W. Jastrzebski, G. Modugno, G. Roati, and A. Simoni, *Phys. Rev. Lett.* **89**, 053202 (2002).
  - [20] G. Modugno, M. Modugno, F. Riboli, G. Roati, and M. Inguscio, *Phys. Rev. Lett.* **89**, 190404 (2002).
  - [21] G. Thalhammer, G. Barontini, L. De Sarlo, J. Catani, F. Minardi, and M. Inguscio, *Phys. Rev. Lett.* **100**, 210402 (2008).
  - [22] D. J. McCarron, H. W. Cho, D. L. Jenkin, M. P. Köpinger, and S. L. Cornish, *Phys. Rev. A* **84**, 011603(R) (2011).
  - [23] T.-L. Ho and V. B. Shenoy, *Phys. Rev. Lett.* **77**, 3276 (1996).
  - [24] E. Timmermans, *Phys. Rev. Lett.* **81**, 5718 (1998).
  - [25] P. Ao and S. T. Chui, *Phys. Rev. A* **58**, 4836 (1998).

- [26] M. Trippenbach, *J. Phys. B At. Mol. Opt. Phys.* **33** (2000).
- [27] R. A. Barankov, *Phys. Rev. A* **66**, 013612 (2002).
- [28] B. Van Schaeybroeck, *Phys. Rev. A* **78**, 023624 (2008).
- [29] S. Gautam and D. Angom, *J. Phys. B* **43**, 095302 (2010).
- [30] D. Gordon and C. M. Savage, *Phys. Rev. A* **58**, 1440 (1998).
- [31] J. G. Kim and E. K. Lee, *Phys. Rev. E* **65**, 066201 (2002).
- [32] X.-L. Li, X.-Y. Yang, N. Tang, L. Song, Z.-K. Zhou, J. Zhang, and Y.-R. Shi, *New J. Phys.* **21**, 103046 (2019).
- [33] J. Han and M. Tsubota, *Phys. Rev. A* **99**, 033607 (2019).
- [34] T. Mithun, K. Kasamatsu, B. Dey, and P. G. Kevrekidis, *Phys. Rev. A* **103**, 023301 (2021).
- [35] M. T. Wheeler, H. Salman, and M. O. Borgh, *Europhys. Lett.* **135**, 30004 (2021).
- [36] A. Richaud, G. Lamporesi, M. Capone, and A. Recati, *Phys. Rev. A* **107**, 053317 (2023).
- [37] A. Bezett, V. Bychkov, E. Lundh, D. Kobayakov, and M. Marklund, *Phys. Rev. A* **82**, 043608 (2010).
- [38] K. Sasaki, N. Suzuki, D. Akamatsu, and H. Saito, *Phys. Rev. A* **80**, 063611 (2009).
- [39] D. Kobayakov, A. Bezett, E. Lundh, M. Marklund, and V. Bychkov, *Phys. Rev. A* **89**, 013631 (2014).
- [40] H. Kadau, M. Schmitt, M. Wenzel, C. Wink, T. Maier, I. Ferrier-Barbut, and T. Pfau, *Nature (London)* **530**, 194 (2016).
- [41] K.-T. Xi, T. Byrnes, and H. Saito, *Phys. Rev. A* **97**, 023625 (2018).
- [42] H. Kokubo, K. Kasamatsu, and H. Takeuchi, *Phys. Rev. A* **104**, 023312 (2021).
- [43] T. Frisch, Y. Pomeau, and S. Rica, *Phys. Rev. Lett.* **69**, 1644 (1992).
- [44] K. Sasaki, N. Suzuki, and H. Saito, *Phys. Rev. Lett.* **104**, 150404 (2010).
- [45] W. J. Kwon, J. H. Kim, S. W. Seo, and Y. Shin, *Phys. Rev. Lett.* **117**, 245301 (2016).
- [46] G. W. Stagg, N. G. Parker, and C. F. Barenghi, *J. Phys. B* **47**, 095304 (2014).
- [47] S. Musser, D. Proment, M. Onorato, and W. T. M. Irvine, *Phys. Rev. Lett.* **123**, 154502 (2019).
- [48] G. W. Stagg, R. W. Pattinson, C. F. Barenghi, and N. G. Parker, *Phys. Rev. A* **93**, 023640 (2016).
- [49] G. W. Stagg, N. G. Parker, and C. F. Barenghi, *Phys. Rev. A* **94**, 053632 (2016).
- [50] G. Gauthier, I. Lenton, N. M. Parry, M. Baker, M. J. Davis, H. Rubinsztein-Dunlop, and T. W. Neely, *Optica* **3**, 1136 (2016).
- [51] K. Sasaki, N. Suzuki, and H. Saito, *Phys. Rev. A* **83**, 033602 (2011).
- [52] M. T. Reeves, T. P. Billam, B. P. Anderson, and A. S. Bradley, *Phys. Rev. Lett.* **114**, 155302 (2015).
- [53] S. J. Rooney, P. B. Blakie, B. P. Anderson, and A. S. Bradley, *Phys. Rev. A* **84**, 023637 (2011).
- [54] This corresponds to a choice of atom number in dimensionless units; that is  $N_1 = L_x L_y - N_2$ , where  $L_x$  and  $L_y$  are the grid sizes in the  $x$  and  $y$  direction, respectively. In order to recover the true atom numbers, this normalization should be multiplied by  $\ell / (a_s \sqrt{8\pi})$ , where  $a_s$  is the  $s$ -wave scattering length, and  $\ell = \sqrt{\hbar / m\omega_z}$  is the harmonic oscillator length in the  $z$  direction associated with a trapping frequency  $\omega_z$ .
- [55] G. R. Dennis, J. J. Hope, and M. T. Johnsson, *Comput. Phys. Commun.* **184**, 201 (2013).
- [56] C. F. Barenghi and N. G. Parker, *A Primer on Quantum Fluids* (Springer, Berlin, 2016).
- [57] P. Nozieres and D. Pines, *The Theory of Quantum Liquids* (Perseus Books, Cambridge, 1999).
- [58] S. Rica, *Physica D (Amsterdam)* **148**, 221 (2001).
- [59] C. Josserand, Y. Pomeau, and S. Rica, *Physica D (Amsterdam)* **134**, 111 (1999).
- [60] T. Winiecki, J. F. McCann, and C. S. Adams, *Phys. Rev. Lett.* **82**, 5186 (1999).
- [61] See Supplemental Material at <http://link.aps.org/supplemental/10.1103/PhysRevLett.133.093403> for additional information on our governing equations, details on our analytic estimate of surface tension and the form of the superfluid Weber number, and example movies of our simulations.
- [62] R. Onofrio, D. S. Durfee, C. Raman, M. Köhl, C. E. Kuklewicz, and W. Ketterle, *Phys. Rev. Lett.* **84**, 810 (2000).
- [63] C. F. Barenghi, *Physica D (Amsterdam)* **237**, 2195 (2008).
- [64] G. Moon, W. J. Kwon, H. Lee, and Y. I. Shin, *Phys. Rev. A* **92**, 051601(R) (2015).